Hybrid Additive Manufacturing of Collector Coins

**João P. M. Pragana [1], Stephan Rosenthal [2], Ivo M. F. Bragança [3], Carlos M. A. Silva [1] ,
A. Erman Tekkaya [2] and Paulo A. F. Martins [1,*]**

[1]   IDMEC, Instituto Superior Técnico, Universidade de Lisboa, 1649-004 Lisboa, Portugal;
joao.pragana@tecnico.ulisboa.pt (J.P.M.P.); carlos.alves.silva@tecnico.ulisboa.pt (C.M.A.S.)

[2]   Institute of Forming Technology and Lightweight Components, TU Dortmund University, Baroper Str. 303,
D-44227 Dortmund, Germany; stephan.rosenthal@iul.tu-dortmund.de (S.R.);
erman.tekkaya@iul.tu-dortmund.de (A.E.T.)

[3]   CIMOSM—Centro de Investigação em Modelação e Optimização de Sistemas Multifuncionais,
ISEL—Instituto Superior de Engenharia de Lisboa, Rua Conselheiro Emídio Navarro, 1, 1959-007 Lisboa,
Portugal; ibraganca@dem.isel.pt

*   Correspondence: pmartins@tecnico.ulisboa.pt

check for
updates

Abstract: The objective of this paper is to present a new hybrid additive manufacturing route for fabricating collector coins with complex, intricate contoured holes. The new manufacturing route combines metal deposition by additive manufacturing with metal cutting and forming, and its application is illustrated with an example consisting of a prototype coin made from stainless steel AISI 316L. Experimentation and finite element analysis of the coin minting operation with the in-house computer program i-form show that the blanks produced by additive manufacturing and metal cutting can withstand the high compressive pressures that are attained during the embossing and impressing of lettering and other reliefs on the coin surfaces. The presentation allows concluding that hybrid additive manufacturing opens the way to the production of innovative collector coins with geometric features that are radically different from those that are currently available in the market.

Keywords: hybrid manufacturing; additive manufacturing; coin minting; experimentation; finite element simulation

1. Introduction

The term "hybrid manufacturing" (HM) started to be used in the late 1990s and has roots in the utilization of primarily processed raw metallic materials in the form of ingots, plates, sheets, rods, tubes, profiles and powders. The use of the term has evolved over the years and is nowadays associated with both concurrent and sequential visions of HM. A concurrent vision of HM requires processes with two or more energy sources/tools having a synergic effect in the processing zone to be combined in situ at the same time. The sequential vision of HM requires the synergic effect in the processing zone to be obtained by a controlled combination of processes acting separately in order to fabricate parts in a more efficient and productive way [1].

A revisitation of the above-mentioned visions of HM by Pragana et al. [2] led to a modification of the original classification of Lauwers et al. [1] to include innovative hybrid additive manufacturing (HAM) routes that make use of deposited metals and are based on the combination of additive and traditional manufacturing processes (Figure 1).
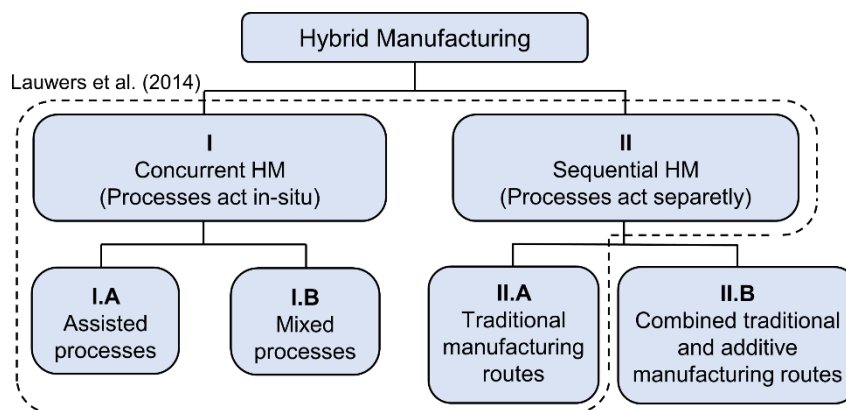
Figure 1. Extended classification of hybrid manufacturing (HM) to include hybrid additive manufacturing (HAM) routes (adapted from Pragana et al. [2]).

The combination of additive and traditional manufacturing processes in metalworking is not new and started back in the mid-1990s when Fessler et al. [3] and Klock et al. [4] combined a laser direct energy deposition (L-DED) system (coupled with a powder feeding system) with a high-speed milling machine to perform metal cutting at intermediate stages of metal deposition.

The integration of additive manufacturing and metal forming processes is more recent (began in the 2010s) and aims to fulfill the following four main objectives; (i) increase the workability domain of additive manufacturing by overcoming its limitations associated with low productivity, metallurgical defects, rough surface quality and lack of dimensional accuracy [5–7], (ii) add flexibility and reduce the amount of material wastage in traditional metal forming processes [8–10], (iii) improve the metallurgical and mechanical properties of the deposited metals during and at the end of a manufacturing route [11–14] and (iv) enable the fabrication of complex tools and tool parts that cannot be manufactured by conventional subtractive methods due to technical and/or economic constraints [15].

This paper presents a new HAM route for producing collector coins that combines metal deposition by additive manufacturing with metal cutting and metal forming. Additive manufacturing with a laser powder bed fusion (LPBF [16,17]) system is first utilized to construct cylinders of deposited metal by sweeping the geometry of the blanks along their thickness direction axis. Then, wire electro-discharge machining (wire-EDM) and polishing are used to slice and prepare the surfaces of the individual coin blanks (hereafter named as "blanks"). Coining in a press-tool system is finally used to embossing and impressing of lettering and other reliefs on the coin surfaces (Figure 2).

The new HAM route allows fabricating collection coins with complex, intricate contoured holes containing the following geometrical features that are difficult (or even impossible) to obtain in conventional wrought blanks by means of blanking, laser cutting, water jet or wire-EDM: (i) very small holes (like the triangle with a side length of 0.4 mm in the eyes of the eagle–refer to "A" in Figure 2a), (ii) tears ("B") with very small angles inside two adjacent sides, (iii) overhang corners ("C") that are not connected to the remaining geometry of the blanks and (iv) small bridges ("D") between the center and the outer regions of the blanks.

If blanking were used, punches and dies would likely fail by fracture when attempting to cut very small holes and tears with small inside angles. The minimum allowable diameter hole in laser cutting is typically 20% of the sheet thickness, meaning that for a blank with 2 mm-thickness, the diameter hole should be larger than 0.4 mm. This value is equal to that required for the eyes of the eagle in the prototype coin, but the tears with small inside angles would create problems for the laser beam to accurately move and cut along two adjacent sides that are almost coincident. A water jet is also not appropriate because the process is not capable of producing accurate holes below 2.5 mm in diameter. Wire-EDM requires the contours of each blank to be produced individually (blank-by-blank), increasing the overall production time and cost compared to that of the new proposed hybrid additive

manufacturing (HAM) route. Moreover, geometrical features like the eyes of the eagle are simply not possible to be obtained by wire-EDM.
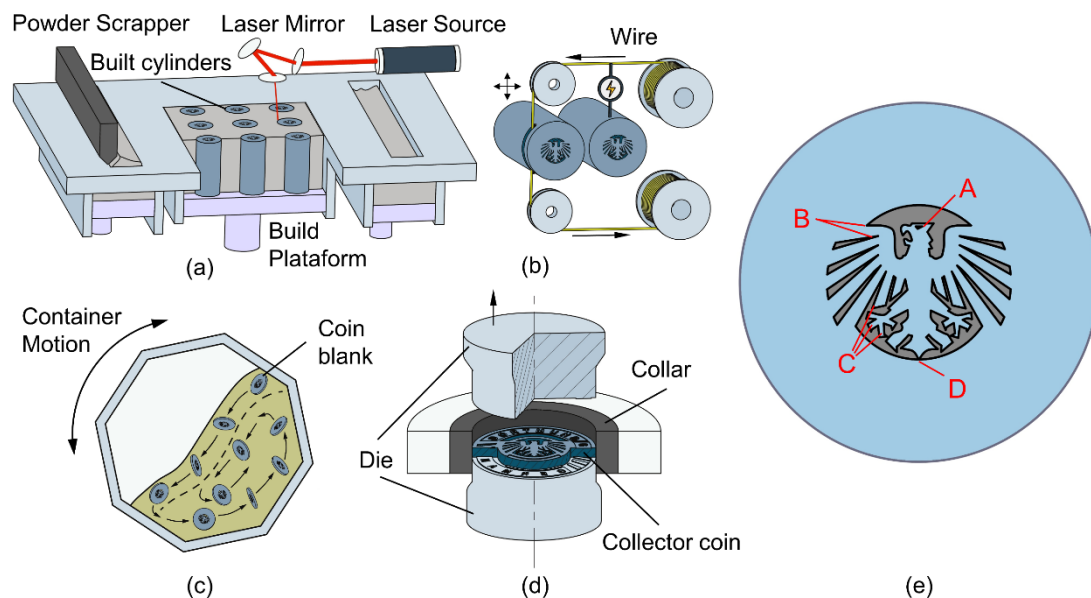

Figure 2. New hybrid additive manufacturing (HAM) route to produce collector coins showing the integration of (**a**) laser powder bed fusion with (**b**) wire electro-discharge machining (wire-EDM), (**c**) polishing and (**d**) coin minting. A prototype coin with details of its major geometrical features is shown in (**e**), where the label "A" refers to very small holes, "B" to tears with very small angles, "C" to overhang corners and "D" to small bridges between the center and the outer regions of the blanks.

Under these circumstances, this paper draws from the fabrication of blanks with complex, intricate contoured holes by a combination of additive manufacturing, wire-EDM and polishing to the analysis of the feasibility of minting these blanks in conventional press-tool systems. Experimentation and finite element modeling of coin minting follow recent publications in the field aimed at analyzing the progressive embossing and impressing of lettering and other reliefs, the evolution of the force with die stroke [18–20] and the maximum bending moment transmitted to the press-tool system derived from misalignment of the resultant vertical force at the end of coin minting [21]. The finite element models utilized in the investigation consider, for the first time ever, the initial porosity of the additively deposited metal by considering the porous blanks as a continuum medium with an initial relative density smaller than that of similar wrought (fully dense) blanks.

2. Materials and Methods

2.1. Additive Manufacturing

The blanks and the compression test specimens were obtained from cylinders with 27.5 mm-diameter (including a 0.25 mm machining allowance) and 60 mm height that was constructed by deposition of AISI 316L stainless steel powder using a DMG Mori Lasertec 30SLM 2nd Gen. machine equipped with a 600 W laser (Figure 3). The main parameters utilized in the deposition are given in Table 1.

Table 1. Main parameters utilized in the fabrication of the blanks and cylindrical test specimens of AISI 316L by laser powder bed fusion.

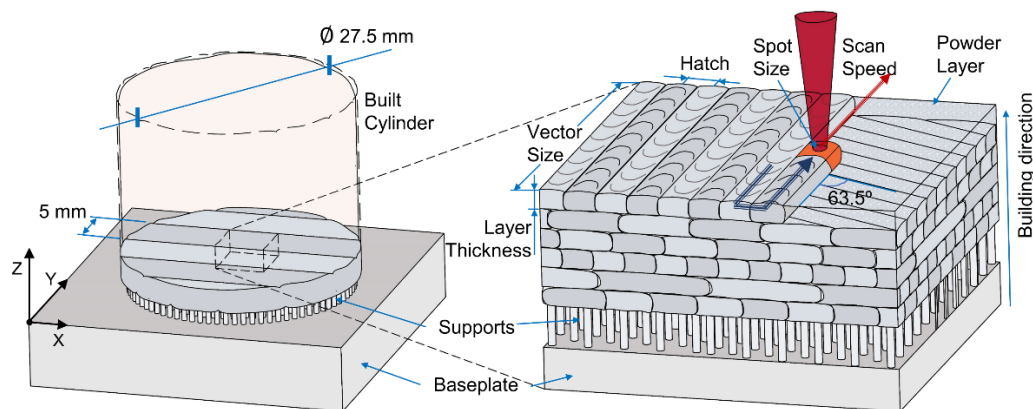| Laser Power (W)	Spot Size (µm)	Scan Speed (mm/s)	Layer Thickness (µm)	Hatch Spacing (µm)	Vector Size (mm)	Shielding Gas
250	100	750	50	100	5	Argon

Figure 3. Deposition strategy utilized in the fabrication of the blanks and cylindrical test specimens of AISI 316L by laser powder bed fusion.

The deposition strategy is schematically illustrated in Figure 3 and consisted of a parallel bi-direction sectorial scanning with 5 mm width, rotated by 63.5° between layers to avoid repetition until several layers are added. This deposition strategy is similar to another with rotation angles of 67° that was recently used by the authors for a different application [22].

Wire electro-discharge machining (wire-EDM) using a (Charmilles Robofil 190) with a wire diameter of 0.25 mm to slice the deposited cylinders into individual blanks. A Struers LabPol-30 polishing machine was utilized for improving the surface finishing of the blanks with fine-grit sandpapers (600 to 2000-grit) and diamond suspensions of 6 and 1 μm (Figure 4).
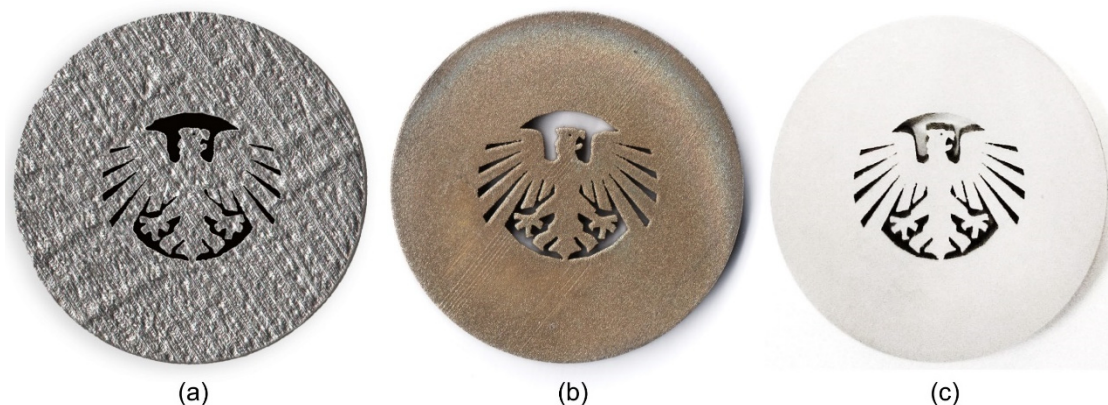

(a) (b) (c)

Figure 4. Photographs of the additively manufactured blanks: (**a**) the constructed cylinder's end; (**b**) the blank sliced from the constructed cylinder by wire-EDM; (**c**) the blank sliced from the constructed cylinder by wire-EDM and polished.

2.2. Testing Procedures

2.2.1. Relative Density

The initial and final average densities of the blanks and coins were determined in a laboratory precision balance (Sartorius 410 BP 410S) equipped with a density determination kit. The testing procedure was based on Archimedes' principle, and a wrought (fully dense) blank made from an AISI 316L stainless steel rod was utilized for reference purposes. The average density of the wrought AISI 316L stainless steel allowed determining the average relative densities R that are included in Table 2. The obtained values are very close to unity and are typical of material deposition by laser powder bed fusion [22].

Table 2. Average and relative densities of the blanks and coins. The wrought blank is included for reference purposes.

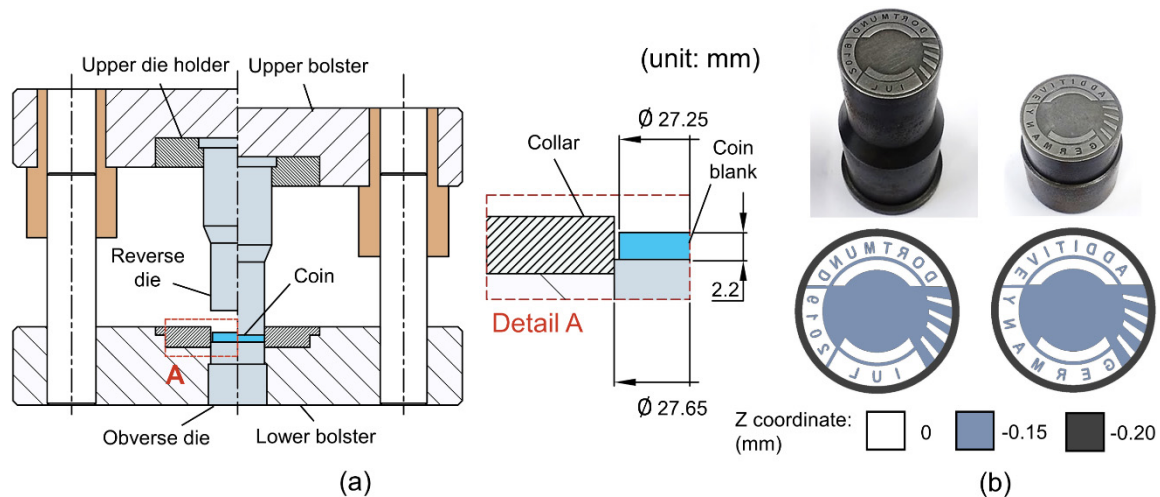|	Wrought Blank	HAM Blank	HAM Coin
Density (g/cm^3)	7967	7937	7953
Relative density R	1	0.996	0.998

2.2.2. Flow Curve

The flow curve of the deposited material was determined by means of compression tests. The specimens were cut out from the constructed cylinders along three different directions (x, y and z) and tested on a hydraulic testing machine with a crosshead speed equal to 10 mm/min.

The compression tests were carried out at room temperature, and the differences in the stress responses along the three different directions (x, y and z) are negligible. This observation confirmed that the deposited metal is isotropic and allowed expressing the average flow curve resulting from the compression tests through the following Ludwik–Hollomon hardening relationship:

$$\sigma_0 = 1325.6 \ \varepsilon^{0.26} \ (MPa) \tag{1}$$

2.2.3. Coin Minting

Coin minting tests were carried out in a press-tool system designed by the authors and installed on the same hydraulic testing machine where the compression tests were done. The tool consists of two (upper and lower) bolsters, an upper die holder, a pair of reverse and obverse dies, and a collar with an inner flat surface (Figure 5a). The dies were made from an AISI D3 cold work steel that was heat treated by hardening and tempering to give a hardness of 60 HRc. The collar was made of tungsten carbide.

Figure 5. (**a**) Press-tool system utilized in the coin minting experiments; (**b**) details of the upper and lower dies.

The dies were designed with a central recess of 0.15 mm in the reverse and obverse die surfaces, as shown in Figure 5b.

Two different types of tests were carried out. In the first type of test (incomplete coin minting), the blanks were compressed up to different preset values of stroke in order to monitor the progressive embossing and impressing of lettering and other reliefs on the coin surfaces. In the second type of test (complete coin minting), the blanks were compressed up to the end of the stroke in order to replicate the coin minting operation by a single strike. Five repetitions were made for each type of test.

2.3. Numerical Modeling

Numerical modeling of coin minting was performed with the in-house finite element computer program i-form [23]. The program is based on the finite element flow formulation [24], and the models utilized in the simulation considered the deposited blanks as a continuum medium with an initial average relative density $R < 1$ (refer to Section 2.2.1).

The finite element formulation is based on the weak form of Markov's rate of energy variational statement applied to the plastic deformation of porous metals, given by,

$$\int_V \overline{\sigma}_R \delta \dot{\overline{\varepsilon}}_R dV - \int_{S_t} t_i \delta u_i dS = 0 \tag{2}$$

where t_i denotes the tractions applied on the boundary S_t, δu_i is an arbitrary variation in the velocity (because the flow formulation is set up in terms of velocities), and $\overline{\sigma}_R$ and $\dot{\overline{\varepsilon}}_R$ are the apparent effective stress and effective strain rate, respectively,

$$\overline{\sigma}_R = \sqrt{AJ_2 + BI_1^2} = \sqrt{C}\,\overline{\sigma}_0 \qquad \dot{\overline{\varepsilon}}_R = \sqrt{\frac{2}{A}D_{ij}'^2 + \frac{1}{3(3-A)}D_V^2} \tag{3}$$

In the above equations, J_2 is the second invariant of the deviatoric stress tensor, I_1 is the first invariant of the stress tensor, $\overline{\sigma}_0$ is the effective stress of the wrought (fully dense) material, D_{ij}' is the deviatoric plastic rate of deformation tensor, $D_V = -\dot{R}/R$ is the volumetric rate of deformation applied to porous metals, and A, B and C are parameters related to the plasticity criterion utilized in numerical modeling (Table 3).

Table 3. Parameters A, B and C of the Doraivelu et al. [25] plasticity criterion as a function of the relative density R of the deposited (porous) metal.

A	B	C
$\left(2 + R^2\right)$	$\left(1 + R^2\right)/3$	$\left(2R^2 - 1\right)$

The constitutive equations for the plastic deformation of porous metals are given by:

$$D_{ij} = \frac{\dot{\overline{\varepsilon}}_R}{\overline{\sigma}_R}\left(\frac{A}{2}\sigma_{ij}' + (3 - A)\sigma_m \delta_{ij}\right) \tag{4}$$

where σ_{ij}' is the deviatoric stress tensor, σ_m is the mean stress and δ_{ij} is the Kronecker delta. In the limiting case of $R = 1$, the volumetric rate of deformation $D_V = 0$, and the Doraivelu et al. [25] plasticity criterion degenerates into the fully dense von Mises plasticity criterion.

The above-described formulation allowed modeling the additively deposited blanks as porous deformable objects and required discretization of their volume by means of nonstructured three-dimensional meshes with approximately 110.000 hexahedral elements (Figure 6).

The discretization made use of four layers of elements across the thickness and a higher density of elements in the outer region where the lettering was impressed, and other details were embossed in-between the wings of the eagle. The dies and collar were modeled as rigid objects and were discretized by means of spatial triangular contact-friction elements.

The central processing unit (CPU) time for a typical finite element simulation was approximately equal to 48 h on a computer equipped with an Intel i7-5930K CPU processor with 6 cores and running an OpenMP (open shared-memory multiprocessing) version of i-form.
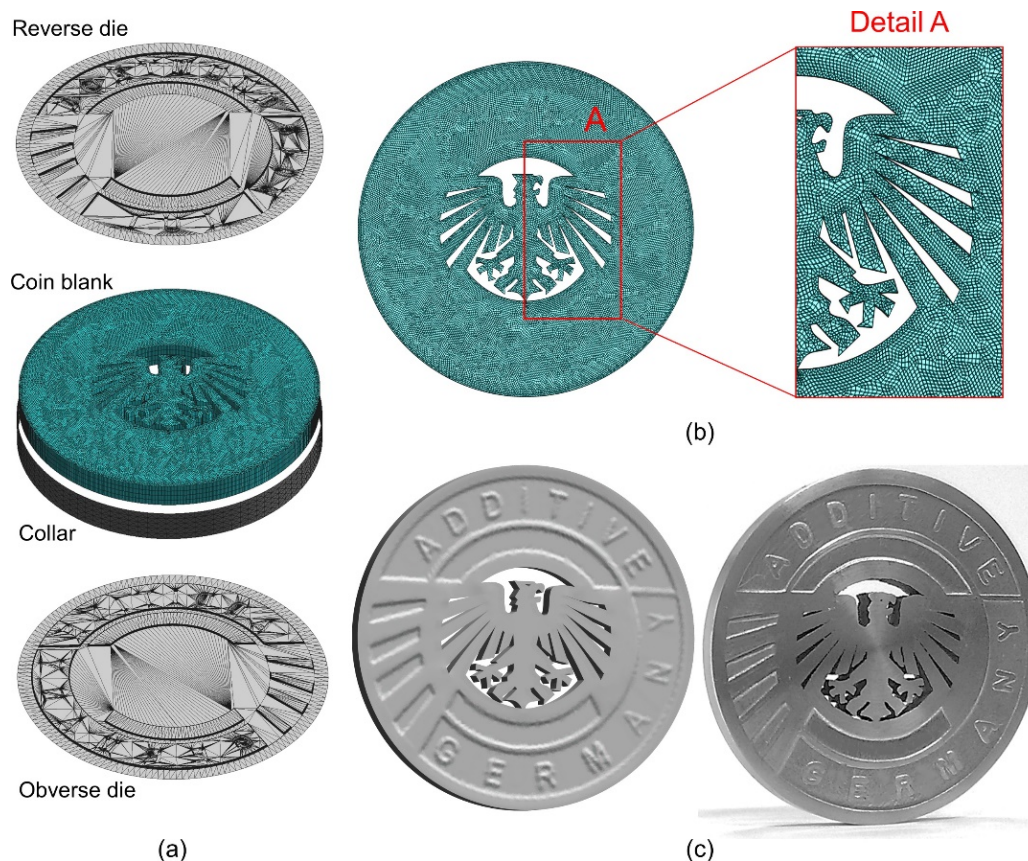
Figure 6. (**a**) Finite element model at the beginning of die stroke; (**b**) top view and detail of the initial mesh; (**c**) computed geometry and photograph of the prototype coin at the end of die stroke.

3. Results and Discussion

3.1. Material Flow

Figure 7 shows the results of the incomplete and complete coin minting tests. In the incomplete tests, the blanks were compressed up 30% and 90% of the total die stroke that is necessary to ensure embossing and impressing of lettering and other reliefs on the coin surfaces.

Observation of the photographs (Figure 7a) in conjunction with the finite-element-predicted distribution of pressure $p = -\sigma_z$ (Figure 7b) allows concluding that contact with the dies starts in the flat region of the outer ring and progressively extends to the lettering. The overall agreement between the actual and the numerically predicted die filling is very good and shows that the center of the coin, containing the eagle and colored in dark red (i.e., with a pressure close to zero), never gets into contact with the dies. This is due to the central recess of 0.15 mm that was created in the reverse and obverse die surfaces (refer to Figure 5b) to prevent distortion of the multiple geometrical features of the eagle.

The finite-element-predicted evolution of relative density given in Figure 7c is compatible with the above-mentioned characteristics of material flow because the relative density increases in the outer ring (as porosity is diminished in this region) and remains practically unchanged in the center of the coin, where there is no contact with the dies. The minimum color scale value in Figure 7c corresponds to approximately 0.025% decrease of the initial relative density and is caused by minor tensile states-of-the-stress that develop at the outer diameter of the coin at the early stages of deformation (i.e., until the coin does not get into contact with the collar).

In case coin minting goes beyond the required total die stroke, there will be contact with the central regions of the reverse and obverse coin surfaces. The "eagle" will deform in accordance with the normalized in-plane velocity vectors $v_{xy}/|v_{die}|$ (Figure 8). However, the analysis of material flow

confirms the excellent ductility of the additively deposited blanks, which allowed fabricating the prototype coins with no signs of incomplete die filling and fracture, even when the recommended die stroke is exceeded.
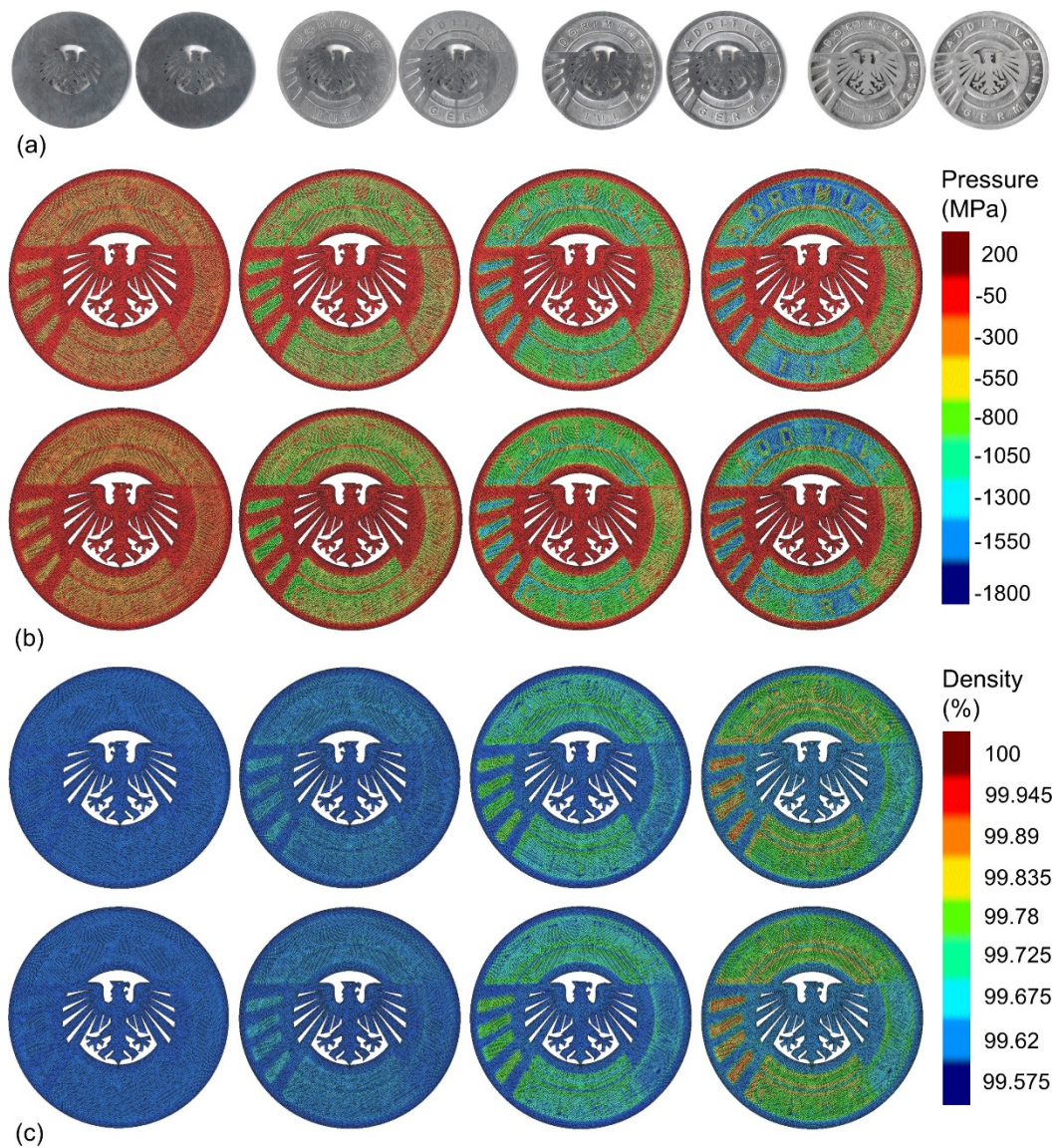

Figure 7. Coin minting of the additively manufactured blanks of AISI 316L stainless steel. (**a**) Photographs; (**b**) finite-element-predicted distribution of pressure (MPa); (**c**) finite-element-predicted distribution of relative density at 0%, 30%, 90% and 100% of the total die stroke.
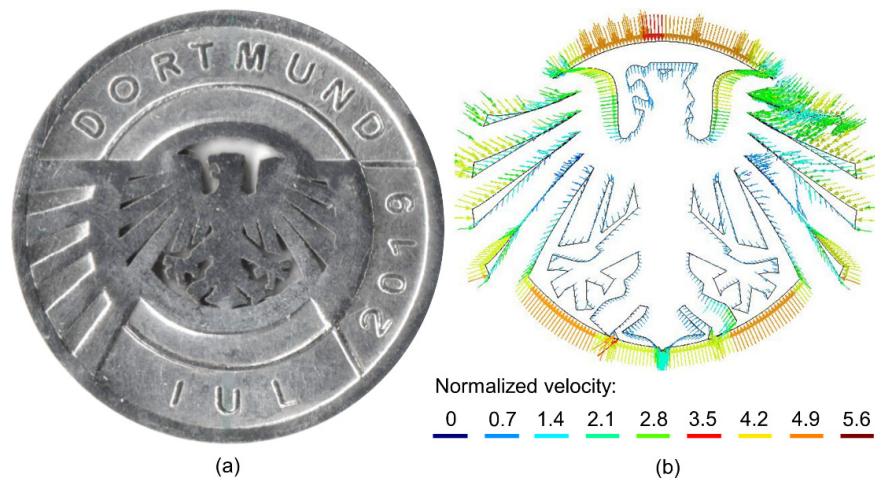
Figure 8. (**a**) Photograph and (**b**) normalized in-plane velocity $v_{xy}/|v_{die}|$ at 150% of the total die stroke.

3.2. Eccentricity of the Vertical Force Resultant

Embossing and impression of lettering and other reliefs on the coin surfaces are responsible for inducing non-symmetric distributions of pressure during coin minting. The lack of symmetry in the pressure gives rise to vertical force resultants that are not aligned with the centerline of the dies and, therefore, to the application of bending moments on the press-tool system. Because these bending moments may create difficulties in die filling and reduce the overall press-tool life, it is important to perform its calculation so that corrections in the design of the coins and dies are made, if necessary, before fabricating the blanks and the dies.

Figure 9 shows the point of application (x, y) of the resultant vertical force at the end of coin minting. As seen, the misalignment towards the centerline of the dies is relatively small and equal to approximately 0.15 mm and 0.21 mm in the x and y directions, respectively. Consequently, the bending moment M resulting from the eccentricity of the vertical force resultant is given by:

$$M = M_x \, \vec{i} + M_y \, \vec{j} = 102.9 \, \vec{i} + 73.4 \, \vec{j} \ \ (N\cdot m) \tag{5}$$

and requires no need to design corrections in both the coins and dies. Design corrections are only relevant for coins giving rise to bending moments above 1000 Nm [21].
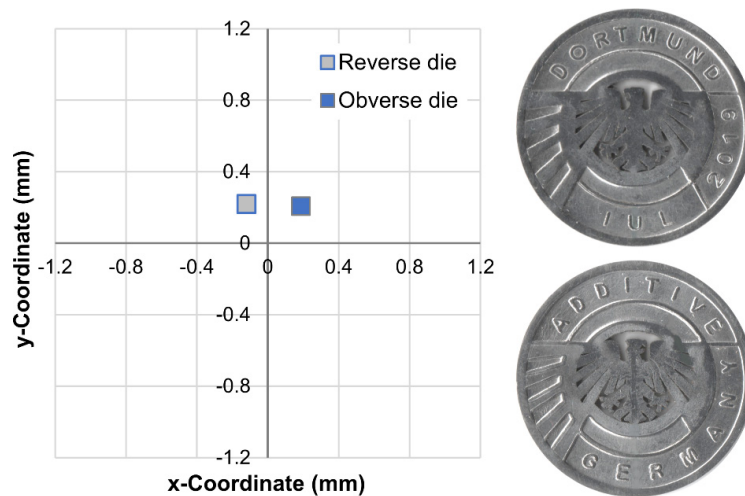

Figure 9. Finite element calculated point of application (x, y) of the resultant vertical force at the end of coin minting in the reverse and obverse dies.

3.3. Force vs. Die Stroke Evolution

A typical force vs. die stroke evolution in coin minting is characterized by an increase of the compression force from zero to high values in the magnitude of hundreds of kN in a few tenths of a millimeter. The experimental and finite element computed evolutions of the force vs. die stroke that were obtained for the prototype coin under investigation exhibit similar trends with four different well-defined stages (Figure 10).
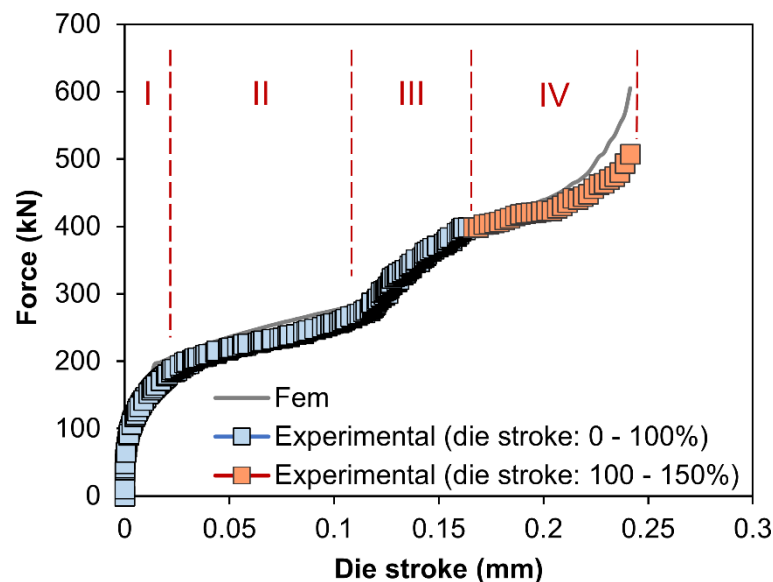

Figure 10. Experimental and finite-element-predicted evolutions of force with die stroke during coin minting of the additively manufactured blanks made AISI 316L stainless steel.

The first stage (labeled as "I") corresponds to a steep increase of the force with die stroke. In this stage, the blank is compressed, and its diameter increases in a free, unconstrained manner until it comes into contact with the inner collar surface. Material flow inside the blank is preferentially directed towards the outside.

In the second stage (labeled as "II"), there is no change in diameter. The material flow starts embossing the regions in between the wings of the eagles and impressing lettering and other reliefs on the reverse and obverse sides of the blanks. As a result of this, the outer regions of the blanks experience some increase of density and progressive elimination of porosity.

The third stage (labeled as "III") corresponds to the end of coin minting. The force increases as the embossing and impressing of lettering and other reliefs are completed, but at a lower rate than that observed in the coin minting of blanks without holes. This is because the contoured holes at the center of the prototype coin prevent material flow from being fully constrained, as in the case of coins without holes. This justifies the relatively small value of force (400 kN) that was required to fabricate the prototype coin—a coin without holes made from the same material would require forces of approximately 1000 kN—and allow concluding that additively manufactured blanks with intricate contour holes are advantageous for prolonging the press-tool life.

The fourth stage (labeled as "IV") corresponds to coin minting beyond the required die stroke. Consequently, the force starts growing at a larger rate and eventually reach values of 600 kN or even more, as the contoured holes of the eagle start to close due to excessive deformation. The excessive deformation of the eagle is the primary reason for setting up a recommended die-stroke for the coin minting operation.

4. Conclusions

Authors proposed a new hybrid additive manufacturing (HAM) route to produce coins with complex, intricate contoured holes. The new manufacturing route replaces conventional fabrication of blanks based on rolling, blanking, edge-trimming and polishing by a new sequence involving material deposition by laser powder bed fusion (LPBF), wire electro-discharge machining and polishing.

The new HAM route has the potential to foster innovation in collection coins by allowing sculptors and designers to utilize shape-optimized blanks with complex geometries that are not easy (or even not possible) to obtain by conventional fabrication methods. The new HAM route also reduces material wastage in the fabrication of blanks.

Coin minting tests in a prototype coin revealed that the additively deposited blanks have good ductility and formability and can easily withstand extreme compressive pressures of approximately 1800 MPa without failure by cracking. The complexity of the contoured holes pays back in preventing material flow to be fully constrained at the end of coin minting and requiring the maximum forces to be significantly smaller than those of the coins without holes. Press-tool life expectancy also increases due to the reduction in force.

The above-mentioned advantages combined with the broader geometry creation capabilities and the possibility of cladding different layers of materials with different colors on top of each other justify the increasingly important role that hybrid additive manufacturing (HAM) will play in the production of small and medium batches of collector coins.

Author Contributions: Investigation, J.P.M.P., S.R., I.M.F.B. and C.M.A.S.; methodology, J.P.M.P., I.M.F.B. and C.M.A.S.; project administration, C.M.A.S.; resources, S.R.; software, J.P.M.P. and P.A.F.M.; supervision, A.E.T. and P.A.F.M.; writing—original draft, J.P.M.P., I.M.F.B.; C.M.A.S. and P.A.F.M.; writing—review and editing, S.R. and A.E.T. and P.A.F.M. All authors have read and agreed to the published version of the manuscript.

Conflicts of Interest: The authors declare no conflict of interest. The funders had no role in the design of the study; in the collection, analyses, or interpretation of data; in the writing of the manuscript, and in the decision to publish the results.

References

1. Lauwers, B.; Klocke, F.; Klink, A.; Tekkaya, A.E.; Neugebauer, R.; Mcintosh, D. Hybrid processes in manufacturing. *Cirp Ann. Manuf. Technol.* **2013**, *63*, 561–583. [CrossRef]
2. Pragana, J.P.M.; Sampaio, R.F.V.; Bragança, I.M.F.; Silva, C.M.A.; Martins, P.A.F. Hybrid metal additive manufacturing: A state-of-the-art review. *Adv. Ind. Manuf. Eng.* **2020**, under review.
3. Fessler, J.R.; Merz, R.; Nickel, A.H.; Prinz, F.B.; Weiss, L.E. Laser Deposition of Metals for Shape Deposition Manufacturing. *1996 International Solid Freeform Fabrication Symposium*. 1996. Available online: http://hdl.handle.net/2152/69928 (accessed on 5 December 2020).
4. Klocke, F.; Wirtz, H.; Meiners, W. Direct Manufacturing of Metal Prototypes and Prototype Tools. *1996 International Solid Freeform Fabrication Symposium*. 1996. Available online: http://hdl.handle.net/2152/69931 (accessed on 5 December 2020).
5. Hölker, R.; Jäger, A.; Ben Khalifa, N.; Tekkaya, A.E. Process and Apparatus for the Combined Manufacturing of Workpieces by Incremental Sheet Metal Forming and Manufacturing Methods in One Set-Up. German Patent DE 10,201414202.7, 2014.
6. Hafenecker, J.; Papke, T.; Huber, F.; Schmidt, M.; Merklein, M. Modelling of hybrid parts made of Ti-6Al-4V sheets and additive manufactured structures. In *Production at the Leading Edge of Technology*; Behrens, B.-A., Brosius, A., Hintze, W., Ihlenfeldt, S., Wulfsberg, J.P., Eds.; Springer: Berlin/Heidelberg, Germany, 2020; pp. 13–22. [CrossRef]
7. Silva, C.M.A.; Bragança, I.M.F.; Cabrita, A.; Quintino, L.; Martins, P.A.F. Formability of a wire arc deposited aluminium alloy. *J. Braz. Soc. Mech. Sci. Eng.* **2017**, *39*, 4059–4068. [CrossRef]
8. Sizova, I.; Bambach, M. Hot workability and microstructure evolution of pre-forms for forgings produced by additive manufacturing. *Procedia Eng.* **2017**, *207*, 1170–1175. [CrossRef]

9. Pragana, J.P.M.; Cristino, V.A.; Bragança, I.M.F.; Silva, C.M.A.; Martins, P.A.F. Integration of forming operations on hybrid additive manufacturing systems based on fusion welding. *Int. J. Precis. Eng. Manuf. Green Technol.* **2019**, 1–13. [CrossRef]

10. Baptista, R.J.S.; Pragana, J.P.M.; Bragança, I.M.F.; Silva, C.M.A.; Alves, L.M.; Martins, P.A.F. Joining aluminium profiles to composite sheets by additive manufacturing and forming. *J. Mater. Proc. Technol.* **2020**, *279*, 116587. [CrossRef]

11. Sokolov, P.; Aleshchenko, A.; Koshmin, A.; Cheverikin, V.; Petrovskiy, P.; Travyanov, A.; Sova, A. Effect of hot rolling on structure and mechanical properties of Ti-6Al-4V alloy parts produced by direct laser deposition. *Int. J. Adv. Manuf. Technol.* **2020**, *107*, 1595–1603. [CrossRef]

12. Colegrove, P.A.; Coules, H.E.; Fairman, J.; Martina, F.; Kashoob, T.; Mamash, H.; Cozzolino, L.D. Microstructure and residual stress improvement in wire and arc additively manufactured parts through high-pressure rolling. *J. Mater. Process. Technol.* **2013**, *213*, 1782–1791. [CrossRef]

13. Maamoun, A.H.; Elbestawi, M.A.; Veldhuis, S.C. Influence of shot peening on AlSi10Mg parts fabricated by additive manufacturing. *J. Manuf. Mater. Process.* **2018**, *2*, 40. [CrossRef]

14. Rosenthal, S.; Platt, S.; Hoelker-Jaeger, R.; Soeren, G.; Kleszczynski, S.; Tekkaya, A.E.; Witt, G. Forming properties of additively manufactured monolithic Hastelloy X sheets. *Mater. Sci. Eng. A* **2019**, *753*, 300–316. [CrossRef]

15. Hoelker, R.; Tekkaya, A.E. Advancements in the manufacturing of dies for hot aluminum extrusion with conformal cooling channels. *Int. J. Adv. Manuf. Technol.* **2015**, *83*, 1209–1220. [CrossRef]

16. Barroqueiro, B.; Andrade-Campos, A.; Valente, R.A.F.; Neto, V. Metal additive manufacturing cycle in aerospace industry: A comprehensive review. *J. Manuf. Mater. Process.* **2019**, *3*, 52. [CrossRef]

17. Moshiri, M.; Candeo, S.; Carmignato, S.; Mohanty, S.; Tosello, G. Benchmarking of laser powder bed fusion machines. *J. Manuf. Mater. Process.* **2019**, *3*, 85. [CrossRef]

18. Xu, J.P.; Liu, Y.Q.; Li, S.Q.; Wu, S.C. Fast analysis system for embossing process simulation of commemorative coin–CoinForm. *Comput. Model. Eng. Sci.* **2008**, *38*, 201–215. [CrossRef]

19. Alexandrino, P.; Leitao, P.J.; Alves, L.M.; Martins, P.A.F. Numerical and experimental analysis of coin minting. *J. Mater. Des. Appl.* **2019**, *233*, 842–849. [CrossRef]

20. Pragana, J.P.M.; Rosenthal, S.; Alexandrino, P.; Araújo, A.; Bragança, I.M.F.; Silva, C.M.A.; Leitão, P.J.; Tekkaya, A.E.; Martins, P.A.F. Coin minting by additive manufacturing and forming. *J. Eng. Manuf.* **2020**. [CrossRef]

21. Alexandrino, P.; Leitão, P.J.; Alves, L.M.; Martins, P.A.F. Finite element design procedure for correcting the coining die profiles. *Manuf. Rev.* **2018**, *5*, 3. [CrossRef]

22. Pragana, J.P.M.; Pombinha, P.; Duarte, V.R.; Rodrigues, T.A.; Oliveira, J.P.; Bragança, I.M.F.; Santos, T.G.; Miranda, R.M.; Coutinho, L.; Silva, C.M.A. Influence of processing parameters on the density of 316L stainless steel parts manufactured through laser powder bed fusion. *J. Eng. Manuf.* **2020**, *234*, 1246–1257. [CrossRef]

23. Nielsen, C.V.; Zhang, W.; Alves, L.M.; Bay, N.; Martins, P.A.F. Coupled Finite Element Flow Formulation. In *Modelling of Thermo-Electro-Mechanical Manufacturing Processes with Applications in Metal Forming and Resistance Welding*; Springer: Berlin/Heidelberg, Germany, 2013. [CrossRef]

24. Tekkaya, A.E.; Martins, P.A.F. Accuracy, reliability, and validity of finite element analysis in metal forming: A user's perspective. *Eng. Comput.* **2009**, *26*, 1026–1055. [CrossRef]

25. Doraivelu, S.M.; Gegel, H.L.; Gunasekera, J.S.; Malas, J.C.; Morgan, J.T.; Thomas, J.F. A new yield function for compressible P/M materials. *Int. J. Mech. Sci.* **1984**, *26*, 527–535. [CrossRef]